Available online at www.sciencedirect.com
SCIENCE DIRECT®
Journal of Solid State Chemistry 177 (2004) 1549–1558
JOURNAL OF SOLID STATE CHEMISTRY
http://elsevier.com/locate/jssc

Non-stoichiometric mixed lead and tin niobates

L.P. Cruz,[a,b] J.-M. Savariault,[c] C.M. Morais,[b] C. Fernandez,[d] J.D. Pedrosa de Jesus,[b] and J. Rocha[b,*]

[a] *Department of Environment, Polytechnique Institute of Viseu, 3510 Viseu, Portugal*
[b] *Department of Chemistry, University of Aveiro, CICECO, 3810-193 Aveiro, Portugal*
[c] *Centre d'Elaboration de Materiaux et d'Etudes Structurales, CNRS B.P. 4347, 31055 Toulouse, Cedex 4 France*
[d] *Laboratoire de Catalyse et Spectrochimie, CNRS-6506, ISMRA/Université de Caen, 14050 Caen, France*

Received 26 August 2003; received in revised form 28 November 2003; accepted 9 December 2003

Abstract

Novel non-stoichiometric mixed lead and tin niobates with the pyrochlore structure have been synthesized via a solid-state route. The materials have been characterized by bulk chemical analysis, single-crystal and powder X-ray diffraction, ^{207}Pb, ^{119}Sn and ^{93}Nb (single and triple quantum) solid-state NMR spectroscopy. The structures of the new non-stoichiometric mixed lead–tin niobate pyrochlore compounds have been Rietveld refined in the cubic system, space group *Fd*-3*m*. The steroactivity of the Sn(II) free electron pair leads to the general formula $(Sn_{1.6-x}Pb_x)(Nb_{2-y}Sn_y)O_{6.6-0.5y}$, where x (0–1.6) is the Pb(II) and y (0–0.34) is the Sn(IV) contents. ^{207}Pb, ^{119}Sn and (in particular) ^{93}Nb NMR support the isomorphous substitution of tin for lead in the compounds studied. ^{93}Nb triple-quantum magic-angle spinning NMR spectroscopy show that the materials contain, at least, two distinct niobium sites, in a 2:1 population ratio, which may be associated with different sample domains.

Keywords: Oxides; Pyrochlore; Niobate; Tin; ^{207}Pb; ^{119}Sn; ^{93}Nb NMR

1. Introduction

The best ferroelectric compounds possess the perovskite structure and most of them contain lead. Although pyrochlore phases are often considered to be undesirable by-products of the perovskite synthesis, Cook and Jaffrey have reported that $Ca_2Nb_2O_7$, a non-centrosymmetric pyrochlore, exhibits ferroelectric properties with spontaneous polarization variable with the electric field [1,2]. The industrial use of lead poses considerable environmental problems and, thus, it is of interest to replace it by a less toxic element. Because many properties of lead(II)-containing compounds are due to the presence of a free electron pair, we attempted to replace lead with tin in niobates with the pyrochlore structure. Pyrochlores are in general described by the formulae AB_2O_6 and $(A_2O')B_2O_6$, while non-stoichiometric pyrochles are expressed by a formula of the type $[A_x(A_2O')_{1-x}]B_2O_6$ [3–6]. Recently, it has been shown that pyrochlores with an A cation possessing a free electron pair cannot be described by the latter formula [5,7].

The only known lead niobate with the pyrochlore structure is non-stoichiometric $Pb_{1.5}Nb_2O_{6.5}$ [8]. Niobates with formula $Pb_{2+x}Nb_2O_{7+x}$ display structures which can be derived from a pyrochlore structure with stacking faults [9]. Recently, we have studied tin niobate compounds and shown that the Sn(II) lone electron pair plays an important role in structure building [10]. Redox reactions did not allow us to determine the upper content of tin which may be introduced in the structure. In the course of this study we have confirmed that Sn(II) is neither in a centric nor axial site as proposed by Birchall and Sleight [11].

In this paper, we wish to report studies on mixed lead and tin niobates of the pyrochlore type. We started this work attempting to prepare a solid solution ranging from $Sn_2Nb_2O_7$ to $Pb_{1.5}Nb_2O_{6.5}$. However, as we shall show, the samples obtained are better described by the formula $(Sn_{1.6-x}Pb_x)(Nb_{2-y}Sn_y)O_{6.6-0.5y}$, where x (0–1.6) is the Pb(II) and y (0–0.34) is the Sn(IV) contents.

*Corresponding author. Fax: +351-234-370084.
E-mail address: rocha@dq.ua.pt (J. Rocha).

0022-4596/$ - see front matter © 2003 Elsevier Inc. All rights reserved.
doi:10.1016/j.jssc.2003.12.010

2. Experimental

2.1. Samples

A series of compounds were obtained by heating mixtures of PbO, SnO and Nb_2O_5 in a sealed silica tube under vacuum (Table 1). The mixture was first grinded in a mortar filled with ethanol, in order to avoid the oxidation of SnO by atmospheric oxygen, and then pressed as a pellet. Grinding and thermal treatments were only performed once because it was found that the extent of the Sn(II) to Sn(IV) oxidation increases with the number of treatments. The thermal treatment conditions were carefully optimized: heating at 850°C for 4 h followed by calcination at 900°C for 2 h. A heating rate of 2°C/min was selected after several tests.

2.2. Techniques

The cells were determined from patterns obtained on a X'Pert MPD Philips diffractometer using Cu$K\alpha$ radiation. The single-crystal determination of sample A1 was described elsewhere [14] and only results were presented here for comparison. The powder XRD data for Rietveld refinement were collected, using Cu$K\alpha$ radiation, on a Seiffert 3000TT diffractometer equipped with a graphite monochromator on the diffracted beam. Densities of selected samples were determined with a Micromeritics AccuPyc1330 helium picnometer and, together with unit cell dimensions, are collected in Table 1. Details on the experimental conditions used for recording the powder XRD patterns are given in Table 2.

^{119}Sn and ^{207}Pb solid-state NMR spectra were recorded at 149.09 and 83.7 MHz, respectively, on a Bruker Avance 400 (9.4 T) spectrometer, while ^{93}Nb (single quantum) NMR spectra were recorded at 122.29 MHz on a Bruker Avance 500 (11.7 T) spectrometer. ^{93}Nb magic-angle spinning (MAS) NMR spectra were recorded on a 2.5 mm Bruker double-bearing probe using a spinning rate of 28 kHz, a 0.6 μs (equivalent to ca. 7°) pulse and a 0.5 s recycle delay. ^{119}Sn solid-state MAS NMR spectra were recorded on a 4 mm double-bearing Bruker probe with a spinning rate of 14 kHz, a 3 μs (equivalent to ca. 50°) pulse and a 30 s optimized recycle delay. Static ^{207}Pb spectra were acquired on a Bruker probe using $\pi/2-\tau-\pi-\tau$ acquired echo pulse sequence, $\tau = 40\,\mu s$, with a 40 s recycle delay. ^{207}Pb MAS NMR spectra were also recorded with MAS (rate 15 kHz) but were found to be similar to the static spectra and, thus, they are not shown here.

The two-dimensional triple-quantum ^{93}Nb MAS NMR experiments were carried out at 122.29 MHz on a Bruker Avance 500 spectrometer, using the z-filter three-pulse sequence. For samples A1 and A5, a 4 mm double-bearing probe was used. The lengths of the first and second hard pulses (radio-frequency magnetic field amplitude $\upsilon_1 = 100$ kHz) were 3.4 and 1.2 μs, respectively. The length of the third soft pulse ($\upsilon_1 = 4$ kHz) was 11.5 μs. The MAS rate was $\upsilon_R = 14$ kHz. Thirty points were acquired in the t_1 domain in increments of $(1/\upsilon_R) = 71.43\,\mu s$. The recycle delay was 0.8 s and 9600 scans were recorded for each t_1 value (total acquisition time per spectrum ca. 2.7 days). For sample A9, a 2.5 mm double-bearing probe was used. The lengths of the first and second hard pulses (radio-frequency magnetic field amplitude $\upsilon_1 = 200$ kHz) were 1.6 and 0.6 μs, respectively. The length of the third soft pulse ($\upsilon_1 = 6$ kHz) was 8.8 μs. The MAS rate was $\upsilon_R = 28$ kHz. Forty-two points were acquired in the t_1

Table 1
Composition of the parent mixtures of oxides, cell parameters and samples densities

Composition	Sample	a (Å)	ρ_{exp} (10^6 g/m^3)
$2SnO + Nb_2O_5$	A1	10.5876(3)	
$1.75SnO + 0.25PbO + Nb_2O_5$	A2	10.5850(4)	6.00(3)
$1.5SnO + 0.5PbO + Nb_2O_5$	A3	10.5773(3)	
$1.25SnO + 0.75PbO + Nb_2O_5$	A4	10.5755(5)	
$1.0SnO + 1.0PbO + Nb_2O_5$	A5	10.5737(5)	6.44(3)
$0.75PbO + 0.75SnO + Nb_2O_5$	A6	10.569(2)	
$0.75SnO + 1.25PbO + Nb_2O_5$	A7	10.5743(4)	6.84(2)
$1.0PbO + 0.5SnO + Nb_2O_5$	A8	10.5713(5)	
$0.5SnO + 1.5PbO + Nb_2O_5$	A9	10.5749(6)	
$1.25PbO + 0.25SnO + Nb_2O_5$	A10	10.571(1)	6.63(1)
$0.25SnO + 1.75PbO + Nb_2O_5$	A11 (1–3)[a]	10.5760(6)	6.97(4)
$1.5PbO + Nb_2O_5$	A12	10.569(1)	6.78(4)

[a] Three different samples have been prepared in separate syntheses.

Table 2
Experimental conditions used for collecting the powder XRD data of each sample for Rietveld refinement

Wavelength	Cu$K\alpha$	$I_{\alpha 2}/I_{\alpha 1} = 0.5$	
Scanning intervals (2θ) (deg)	10–50	50–100	100–160
Measuring time per step (s) for each scan (s)	19	28	37
Scan step (2θ) (deg)	0.02	0.02	0.02
Collimation slits (deg)	2.0	Soller's slits	3.0
Output slits		Soller's slits	0.1
Size of sample	Length 30 mm	Thickness 0.5 mm	
Width of beam	10 mm		

domain in increments of $(1/\nu_R) = 35.71\,\mu s$. The recycle delay was 0.8 s and 9600 scans were recorded for each t_1 value (total acquisition time ca. 3.7 days). The ppm scale of the sheared spectra was referenced to ν_0 frequency in the ν_2 domain and to $0.47\nu_0$ (high-resolution spectra after shearing) in the ν_1 domain. Numerical simulations of the single- and triple-quantum spectra were carried out with the homemade programme MASAI [12]. ^{93}Nb, ^{119}Sn and ^{207}Pb chemical shifts are quoted in ppm from, respectively, solid Nb_2O_5, liquid $Sn(CH_3)_4$ and liquid $Pb(CH_3)_4$.

Bulk chemical analysis by ICP-AES has been performed on a Jobin Yvon JY *plus* spectrometer.

3. Results and discussion

3.1. X-ray diffraction

During the Rietveld analysis, it was found that the profile of diffraction lines could not be fitted by the classical functions available. Close inspection reveals an asymmetric broadening of the pedestal of *all* reflections (Fig. 1). This broadening may be due to: (i) an instrumental problem, due to the energy window selected by the monochromator, which has been ruled out; (ii) the presence of a second (impurity) phase; (iii) a diffuse scattering phenomenon due to a distribution of atoms around a highly symmetric site [13]. The latter is a likely possibility, since in the crystal structure of $Sn_{1.6}Nb_{1.7}O_{6.2}$ tin is pulled out of the center of the tunnel separating two large cavities of the pyrochlore structure [14]. Tin is, thus, distributed over six sites instead of a single one originating a broad diffusion peak around the main powder XRD peak. This can be considered as a signature of Sn(II) outside its normal site, the center of the tunnel, as observed for the corresponding lead compound. On the other hand, because all pyrochlore reflections exhibit a broadening of the pedestal if a second phase is present this is a pyrochlore, which displays very broad (ca. 10 times broader than the main phase) and asymmetric reflections. Hence, both a diffusion phenomenon and the presence of a second phase may explain the broadening of the reflections. The quality (R_f) of these two Rietveld refinements and the refinement carried out not considering any peak broadening is similar (even if the R_P value for each sample decreases 2–3% when peak broadening is considered). This explains why the structures reliability factors are relatively poor. Pseudo-Voigt functions were used to perform Rietveld refinement using FULLPROF [15]. The latter allows the separation of the overlapping reflections according to the model used. The structure factor intensities obtained by this method were introduced in programme SHELXL [16], which allows to constraint electroneutrality, atom geometry, and the use of more than two kinds of atoms in a given site (this is not possible with FULLPROF). The niobium site was assumed to be fully occupied by Nb(V) and Sn(IV). The results obtained with SHELXL were reintroduced in the Rietveld refinement, in order to improve the model. The cycle was repeated until no significant change was observed.

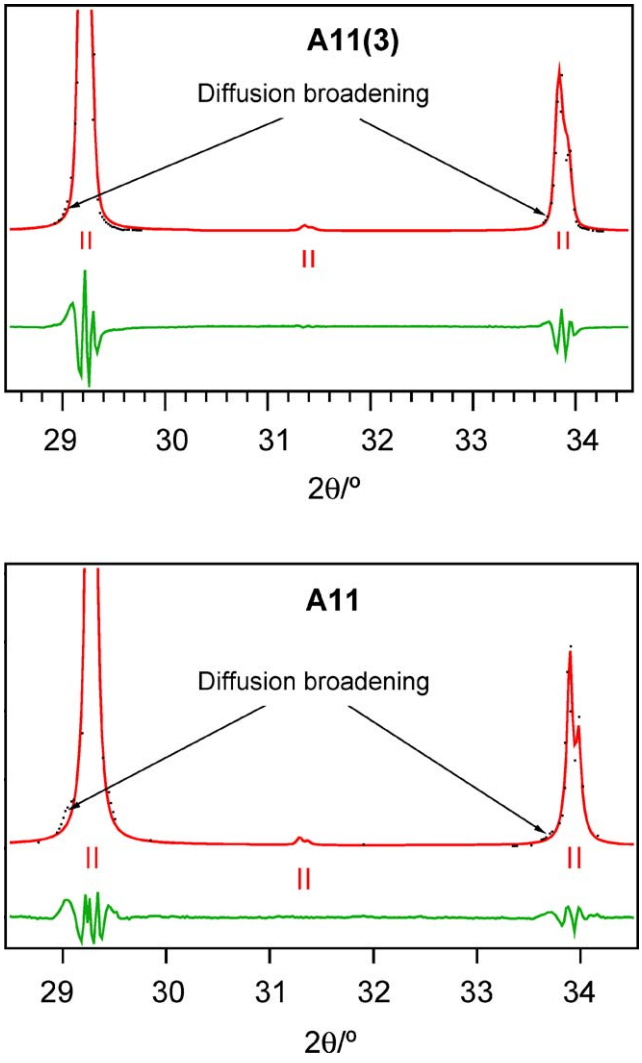

Fig. 1. Selected region of the powder XRD patterns of samples A11(3) and A3 showing peak broadening by diffusion.

The starting positions of the atoms were the classical pyrochlore structure positions using the second set of the space group *Fd*-3*m*, origin at center -3*m*. Tin was introduced as in the tin niobate structure [14], i.e., at the $(0, y, -y)$ site (96 h) (Fig. 2). Attempted refinements with tin in the tunnel center, at the lead position, gave unacceptable results. It has been assumed that no metal is present in the O2 site. Indeed, the relatively high value of the thermal displacement parameter indicates low electron density in this site: using, e.g., the O2 occupation factor (0.66, Table 4) an electron density of

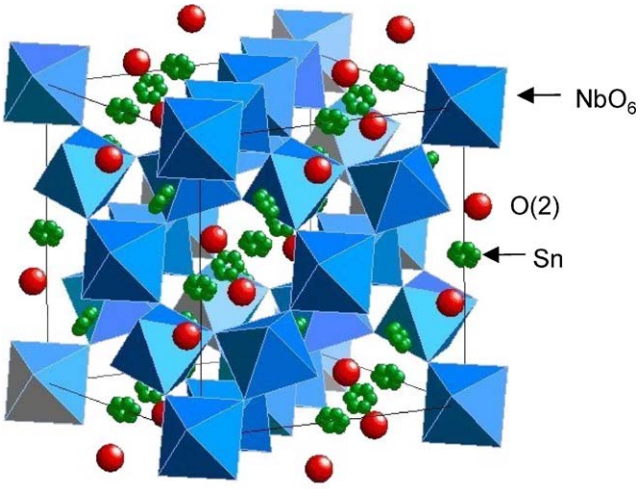

Fig. 2. Schematic view of the pyrochlore structure.

ca. 5.28 is obtained; if, instead, Sn(II) resides in the O2 site the occupation factor is only 0.10.

Careful examination of the XRD pattern reveals the presence of reflections not attributed to a pyrochlore phase. Indexation of these reflections indicates that 1–1.4% metallic lead is present in the compounds and this was taken into account in the Rietveld refinements. The final reliability factors of the refinements are presented in Table 3 while an example of the final profile is shown in Fig. 3. As expected, the reliability factors are not very good but convergence between FULLPROF and SHELXL results lend credit to the solution found.

The A11 cell parameters are identical, indicating that the samples are essentially the same although they have been prepared in different synthesis. Table 4 gathers the final occupation factors and the corresponding number of atoms per formula unit. The main conclusion is the formulae obtained do *not* correspond to $(A_2O')B_2O_6$, but rather $(Sn_{1.6-x}Pb_x)(Nb_{2-y}Sn_y)O_{6.6-0.5y}$, where x (0–1.6) is the Pb(II) and y (0–0.34) is the Sn(IV) contents. In addition, the presence of Sn(IV) and free lead indicates that redox reactions occur involving the classic mechanisms: $2SnO \Leftrightarrow Sn + SnO_2$ and $PbO + Sn \Leftrightarrow Pb + SnO$. The composition found corresponds to the thermodynamic equilibrium at the temperature of the reaction.

The interaction sphere of the Pb(II) and Sn(II) lone electron pairs has been assumed to be as bulky as the oxygen ion. We have already proposed that a competition, to fill in the central cavity (CC), occurs between the lone electron pair and the oxygen O′ [17]. This provides a constraint for the pyrochlore formula. For example, for a pyrochore with a lone pair element (AE)(II), of formula $(AE^{2+})_xNb_2O_{6+y}$ electroneutrality gives

$$2x + 10 - 12 - 2y = 0 \Rightarrow x - y = 1.$$

Table 3
Final Rietveld refinement results and cell parameters

Sample	FULLPROF				a (Å)
	R_p	χ^2	R_{Bragg}	R_f	
A11 (1)	9.83	3.81	7.88	12.08	10.5765(6)
A11 (2)	6.69	2.58	7.40	8.81	10.5757(6)
A11 (3)	7.44	3.21	6.78	7.58	10.5762(1)
A5	6.02	1.77	5.25	9.08	10.5748(8)
A2[a]	9.46	7.8	8.68	6.88	10.5861(2)

[a] Data were truncated at 100°2θ

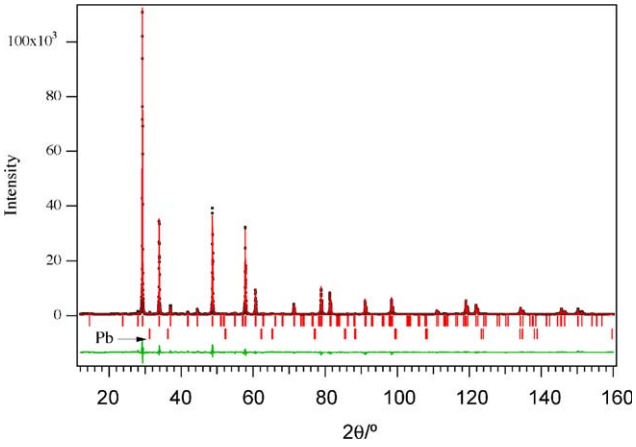

Fig. 3. Experimental and simulated powder XRD patterns of sample A5.

CC occupation leads to the equation:

$x/4 + y = 1$ (assuming a full occupation of the CC site and 4 lone pairs pointing at the CC center, i.e., 4 metals) $\Rightarrow x + 4y = 4$.

The solutions are $x = 1.6$ and $y = 0.6$, and the formula becomes $(AE)_{1.6}Nb_2O_{6.6}$. The introduction of 0.2 atoms of A^{4+} in the niobium site gives a formula $(AE^{2+})_x(Nb_{1.8}A^{4+}_{0.2})O_{6+y}$, the equation becomes

$$2x + 1.8 \times 5 + 0.2 \times 4 - 12 - 2y = 0 \Rightarrow x - y = 1,$$

$$x/4 + y = 1$$

with solutions $x = 1.68$ and $y = 0.58$ and the corresponding formula $(AE^{2+})_{1.68}$ $(Nb_{1.8}A^{4+}_{0.2})O_{6.58}$.

Using this result and the chemical analysis data, experimental formulae were calculated and are given in Table 5. We note that although, for some compounds, the expected and experimental formulae do not entirely agree, the inconsistency may be understood assuming vacancies in CC site (or, in other words, $x/4 + y < 1$). The final atomic coordinates, with the isotropic thermal displacement factors, are given in Table 6. We note that the A2 sample atomic parameters are affected by the data set truncation (data were recorded only up to 100°2θ).

Table 4
Final occupation factors determined using SHELXL and corresponding number of atoms per formula unit

	A11 (1)		A11 (2)		A11 (3)		A5		A2	
	Occup.	N atoms	Occup.	N atoms	Occup.	N atoms	Occup.	N atoms	Occup.	N atoms
Nb1 (16*c*)	0.91(1)	1.82(2)	0.96(1)	1.92(2)	0.91(1)	1.82(2)	0.96(1)	1.92(2)	0.76(1)	1.53(2)
Sn1 (16*c*)	0.09(1)	0.18(2)	0.04(1)	0.08(2)	0.09(1)	0.18(2)	0.04(1)	0.08(2)	0.24(1)	0.47(2)
Pb2 (16*d*)	0.57(2)	1.16(4)	0.60(4)	1.20(9)	0.52(1)	1.03(2)	0.41(1)	0.82(2)	0.12(6)	0.24(13)
Sn2 (96*h*)	0.05(1)	0.58(7)	0.03(1)	0.41(9)	0.05(1)	0.58(8)	0.07(1)	0.80(7)	0.13(2)	1.49(13)
O1 (48*f*)	1	6	1	6	1	6	1	6	1	6
O2 (8*b*)	0.66(5)	0.66(5)	0.58(4)	0.58(4)	0.53(1)	0.53(1)	0.58(1)	0.58(1)	0.50(6)	0.50(6)

Table 5
Chemical composition data and formulae of the tin–lead niobates with the pyrochlore structure

Samples	Calculated formulae	ICP-AES						% vacancies in the site *8b* (CC)	Experimental formulae
		% Sn (m/m)		% Pb (m/m)		% Nb (m/m)			
		Exp.	Calc.	Exp.	Calc.	Exp.	Calc.		
A1	$Sn_{1.6}Nb_2O_{6.6}$	45.05	44.05	—	—	35.40	34.59	0.0	$Sn_{1.67}(II)Nb_{1.84}Sn(IV)_{0.16}O_{6.59}$
A2	$Sn_{1.4}Pb_{0.2}Nb_2O_{66}$	37.33	36.01	9.50	9.33	35.47	34.03	0.0	$Sn_{1.42}(II)Pb_{0.23}Nb_{1.87}Sn(IV)_{0.13}O_{6.59}$
A3	$Sn_{1.2}Pb_{0.4}Nb_2O_{6.6}$	30.70	30.04	17.17	17.22	32.40	32.84	0.0	$Sn_{1.22}(II)Pb_{0.44}Nb_{1.87}Sn(IV)_{0.13}O_{6.59}$
A4	$Sn_{1.0}Pb_{0.6}Nb_2O_{6.6}$	25.04	24.54	25.91	25.18	32.26	31.17	0.0	$Sn_{0.99}(II)Pb_{0.67}Nb_{1.85}Sn(IV)_{0.15}O_{6.59}$
A5	$Sn_{0.8}Pb_{0.8}Nb_2O_{6.6}$	18.78	18.60	32.92	32.11	31.43	30.73	0.0	$Sn_{0.77}(II)Pb_{0.88}Nb_{1.88}Sn(IV)_{0.12}O_{6.59}$
A6	$Sn_{0.75}Pb_{0.75}Nb_2O_{6.5}$	16.40	16.34	29.20	29.32	34.80	34.77	2/8	$Sn_{0.68}(II)Pb_{0.74}Nb_{1.96}Sn(IV)_{0.04}O_{6.40}$
A7	$Sn_{0.6}Pb_{1.0}Nb_2O_{6.6}$	13.16	13.13	39.58	39.13	30.13	29.81	0.0	$Sn_{0.54}(II)Pb_{1.11}Nb_{1.89}Sn(IV)_{0.11}O_{6.59}$
A8	$Sn_{0.5}Pb_{1.0}Nb_2O_{6.5}$	10.50	10.44	38.00	37.55	33.90	33.35	1/8	$Sn_{0.49}(II)Pb_{1.01}Nb_{2.00}O_{6.5}$
A9	$Sn_{0.4}Pb_{1.2}Nb_2O_{6.6}$	8.65	8.74	44.68	45.03	28.46	28.36	5/8	$Sn_{0.06}(II)Pb_{1.18}Nb_{1.66}Sn(IV)_{0.34}O_{6.07}$
A10	$Sn_{0.25}Pb_{1.25}Nb_2O_{6.5}$	4.80	4.82	45.00	45.00	32.30	32.11	2/8	$Sn_{0.19}(II)Pb_{1.23}Nb_{1.96}Sn(IV)_{0.04}O_{6.40}$
A11	$Sn_{0.2}Pb_{1.4}Nb_2O_{6.6}$	4.67	4.65	49.24	50.71	27.20	27.72	1/8	$Sn_{0.07}(II)Pb_{1.5}Nb_{1.83}Sn(IV)_{0.17}O_{6.48}$
A12	$Pb_{1.5}Nb_2O_{6.5}$	—	—	49.36	50.16	31.95	32.13	2/8	$Pb_{1.40}Nb_{2.00}O_{6.40}$

Table 6
Atomic parameters including isotropic thermal displacement parameters

	$Sn_{0.2}Pb_{1.4}Nb_2O_{6.6}$ A11 (1)	$Sn_{0.2}Pb_{1.4}Nb_2O_{6.6}$ A11 (2)	$Sn_{0.2}Pb_{1.4}Nb_2O_{6.6}$ A11(3)	$Sn_{0.8}Pb_{0.8}Nb_2O_{6.6}$ A5	$Sn_{1.4}Pb_{0.2}Nb_2O_{6.6}$ A2
Nb1, Sn1[a]					
B_{iso} (Å^2)	1.7(3)	2.13(3)	2.89(8)	2.61(9)	1.2(5)
O1					
x	0.312(2)	0.3137(5)	0.3109(7)	0.312(2)	0.314(2)
y	1/8	1/8	1/8	1/8	1/8
z	1/8	1/8	1/8	1/8	1/8
B_{iso} (Å^2)	2.0(4)	1.6(1)	1.6(4)	2.3(2)	3.0(7)
Pb2[b]					
B_{iso} (Å^2)	1.9(3)	1.59(2)	1.71(9)	1.06(9)	1.6(6)
Sn2					
x	0	0	0	0	0
y	0.295(2)	0.2979(7)	0.2947(9)	0.296(2)	0.276(3)
z	−0.295(2)	−0.2979(7)	−0.2947(9)	−0.296(2)	−0.276(3)
B_{iso} (Å^2)	1.7(5)	1.3(2)	1.5(4)	2.3(2)	1.1(6)
O2[c]					
B_{iso} (Å^2)	3.3(7)	2.3(7)	2.7(7)	2.3(3)	6.2(6)

[a] Nb1 and Sn1 located in site 16c have coordinates 0, 0, 0.
[b] Pb2 located in site 16d has coordinates 0.5, 0.5, 0.5.
[c] O2 located in site 8b has coordinates 3/8, 3/8, 3/8.

Table 7
Selected bond distances and angles (Å, deg)

	$Sn_{0.2}Pb_{1.4}Nb_2O_{6.6}$ A11(1)	$Sn_{0.2}Pb_{1.4}Nb_2O_{6.6}$ A11(2)	$Sn_{0.2}Pb_{1.4}Nb_2O_{6.6}$ A11(3)	$Sn_{0.8}Pb_{0.8}Nb_2O_{6.6}$ A5	$Sn_{1.4}Pb_{0.2}Nb_2O_{6.6}$ A2
Nb1–O1 × 6	1.980(2)	1.987(2)	1.978(2)	1.982(6)	1.990(6)
Pb2–O2 × 2	2.2899(4)	2.2897(4)	2.2898(5)	2.2895(8)	2.2919(8)
Pb2–O1 × 6	2.732(4)	2.716(4)	2.738(5)	2.73(1)	2.72(1)
Sn2–O2 × 2	2.388(6)	2.399(6)	2.385(8)	2.39(2)	2.33(2)
Sn2–O1 × 2	2.180(7)	2.134(6)	2.191(9)	2.17(2)	2.39(3)
Sn2–O1 × 2	2.815(6)	2.809(6)	2.818(8)	2.81(2)	2.74(2)
Sn2–O1 × 2	3.331(7)	3.351(7)	3.33(1)	3.34(2)	3.06(3)
Nb1–Pb2 × 6	3.739(1)	3.739(1)	3.739(1)	3.739(1)	3.742(2)
Nb1–Sn2 × 1	3.06(2)	3.022(7)	3.071(9)	3.05(2)	3.35(3)
Nb1–Sn2 × 2	3.45(1)	3.437(4)	3.454!6)	3.45(1)	3.56(2)
Nb1–Sn2 × 2	4.12(2)	4.144(5)	4.114(7)	4.13(1)	3.95(2)
Nb1–Sn2 × 1	4.42(2)	4.456(7)	4.407(9)	4.43(2)	4.14(3)
O1–Nb1–O1	90.4(2)	90.5(2)	90.6(3)	90.1(6)	90.6(6)
O1–Nb1–O1	89.6(2)	89.5(2)	89.4(3)	89.9(6)	89.4(6)
O2–Pb2–O1	97.91(7)	98.23(7)	97.8(1)	98.0(2)	98.3(2)
O2–Pb2–O1	82.09(7)	81.77(7)	82.2(1)	82.0(2)	81.7(2)
O1–Pb2–O1	61.86(3)	62.01(3)	61.82(5)	61.9(1)	62.0(1)
O1–Pb2–O1	118.14(3)	117.99(3)	118.18(5)	118.1(1)	118.0(1)
O1–Sn2–O1	80.2(2)	81.9(3)	79.8(3)	80.7(7)	71.8(8)
O1–Sn2–O2	112.5(3)	113.5(3)	112.2(4)	112.8(8)	107.(1)
O1–Sn2–O2	92.9(2)	93.0(2)	93.0(2)	93.0(5)	96.7(3)
O1–Sn2–O1	67.1(1)	67.4(1)	67.0(2)	67.1(3)	65.7(5)
O1–Sn2–O1	139.3(3)	140.4(3)	139.0(4)	139.6(8)	130.(1)
O1–Sn2–O1	164.8(2)	163.7(2)	165.1(2)	164.5(5)	171.3(7)
O2–Sn2–O2	147.1(3)	145.2(3)	147.5(4)	146.6(8)	161.(1)
O2–Sn2–O1	78.7(2)	78.0(2)	78.9(3)	78.5(6)	74.0(7)
O2–Sn2–O1	93.4(1)	93.2(1)	93.5(1)	93.4(3)	88.6(9)
O2–Sn2–O1	81.4(2)	80.8(2)	81.6(3)	81.2(5)	80.5(9)
O2–Sn2–O1	68.6(2)	67.5(2)	68.8(2)	68.3(4)	71.8(8)
O1–Sn2–O1	152.2(3)	150.4(3)	152.6(4)	151.7(7)	164.(1)
O1–Sn2–O1	53.6(1)	53.2(1)	53.7(1)	53.5(3)	57.4(4)
O1–Sn2–O1	99.0(2)	97.8(2)	99.4(3)	98.7(5)	106.5(9)
O1–Sn2–O1	49.9(1)	49.4(1)	50.0(1)	49.7(3)	54.5(5)

The coordinates found for the three A11 samples ($Sn_{0.2}Pb_{1.4}Nb_2O_{6.6}$) studied set a range of uncertainty for the measurements. Comparison with the corresponding coordinates of other compounds shows that the pyrochlore structure is very difficult to deform.

Selected inter-atomic distances and angles are given in Table 7. The niobium surrounding is very similar in all compounds. This is due to the fact that the number of tin atoms substituting for niobium in each compound is very small and, thus, niobium imposes its weight on the diffraction phenomenon. On the other hand, the distance Nb–O is similar to the distance observed for $Sn_{1.7}Nb_{1.7}O_{6.2}$ crystals, i.e., a weighted average between pure Nb–O and Sn(IV)–O distances [17]

$$d\mathrm{B{-}O} = [(2-x)\,d(\mathrm{Nb{-}O})/Z_{\mathrm{Nb}} + x\,\mathrm{d}(\mathrm{Sn{-}O})/Z_{\mathrm{Sn}}]/[(2-x)/Z_{\mathrm{Nb}} + x/Z_{\mathrm{Sn}}].$$

where Z is the atomic number. Using an average x of 0.2 the calculated $d(B\text{–O})$ is 1.976 Å, similar to the experimental values. Valence calculations [18] confirm the presence of Sn(IV) and Nb(V) in the same site (Table 8).

The lead surrounding appears to be of the type 6O1 + 2O2, forming a cube just like in the $Pb_{1.5}Nb_2O_{6.5}$ compound. The cube is distorted along the O2–Pb–O2 direction, a [110] type axis. The Pb–O2 distances are shorter than the Pb–O1 distances and the angles O2–Pb–O1 are closer to 90° than the O1–Pb2–O1 angles. In the case of Sn2, with a surrounding also of type 6O1 + 2O2, the fact that Sn2 is shifted off the [110] axis adds a new distortion. The Sn2–O1 distances vary from 2.13 to 3.3 Å. This additional distortion is better seen on the O–Sn–O angle: the O2–Sn2–O2 angle is 149(4)° while the corresponding O2–Pb–O2 angle is 180°. One way of determining the surrounding of a metal is to calculate its valence [18]. The results of such calculation are given in Table 8 and for tin and lead the valence does not deviate from the expected value 2. The lower values found for Sn2 in compound A2 are attributed to the lowest precision obtained in the structure determination (high-angle data were lost). But because we have assumed that the lone electron pair of Sn(II) and Pb(II) occupies an O2 site, the surrounding becomes 6O1 + O2, and the

Table 8
Valence of metal atoms

	$Sn_{0.2}Pb_{1.4}Nb_2O_{6.6}$ A11(1)	$Sn_{0.2}Pb_{1.4}Nb_2O_{6.6}$ A11(2)	$Sn_{0.2}Pb_{1.4}Nb_2O_{6.6}$ A11(3)	$Sn_{0.8}Pb_{0.8}Nb_2O_{6.6}$ A5	$Sn_{1.4}Pb_{0.2}Nb_2O_{6.6}$ A2
Nb1	4.25	4.16	4.27	4.23	4.13
Sn2 (6O1 + 2O2)	1.97	2.09	1.94	2.00	1.71
Sn2 (6O1 + 1O2)	1.66	1.79	1.62	1.69	1.33
Pb2 (6O1 + 2O2)	2.17	2.22	2.16	2.19	2.22
Pb2 (6O1 + 1O2)	1.60	1.65	1.59	1.62	1.65

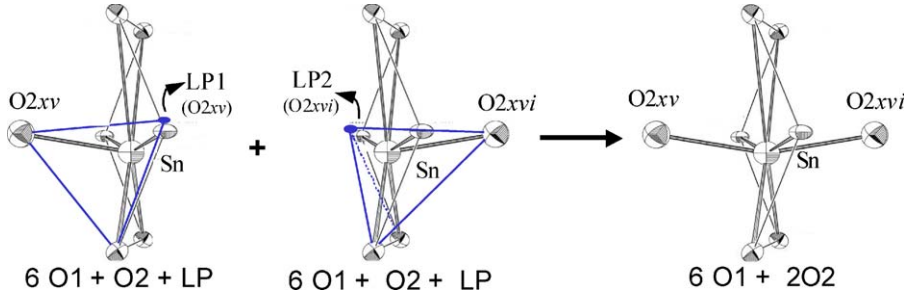

Fig. 4. Local tin environments in $(Sn_{1.6-x}Pb_x)(Nb_{2-y}Sn_y)O_{6.6-0.5y}$ samples.

valence decreases in a drastic way. This may indicate that (i) the surrounding is of the type 6O1 + 2O2, which is contradicted by the chemical analysis and the lone pair position in the structure, or alternatively that (ii) the coordinates of Pb2 and Sn2 are similar, which is not surprising because X-ray diffraction averages positions over the whole crystallite. One must assume that lead does not occupy the CT (center of the tunnel) site, rather it is pulled out towards a CC site, opposite to the lone pair direction. In another site, lead is pulled out in the opposite direction and, hence, the average between these two positions is the center of the tunnel. The same mechanism may be invoked for the tin position, excepted that tin is already shifted from CT, perpendicularly to the [110] direction (Fig. 4).

4. Solid-state NMR

^{119}Sn MAS NMR spectra of selected $(Sn_{1.6-x}Pb_x)(Nb_{2-y}Sn_y)O_{6.6-0.5y}$ samples are shown in Fig. 5. The spectra display a single signal with a full-width-at-half-maximum (FWHM), which increases with increasing tin content from around 35 to 55 ppm. Simultaneously, the peak maximum shifts from ca. −630 to −615 ppm. The increasing line widths may be due to a distribution of chemical shifts brought about by the framework insertion of tin. ^{119}Sn MAS NMR spectra of related compounds have been previously discussed [10]. Although the isotropic chemical shifts are characteristic of Sn(IV) this assignment is not trivial. An important conclusion drawn in Ref. [10] is that it may not be possible to distinguish by this technique six-coordinated Sn(IV) from seven- or eight-coordinated Sn(II), particularly when chemical shift distributions are present and the spectra signal-to-noise (S/N) ratios are relatively poor.

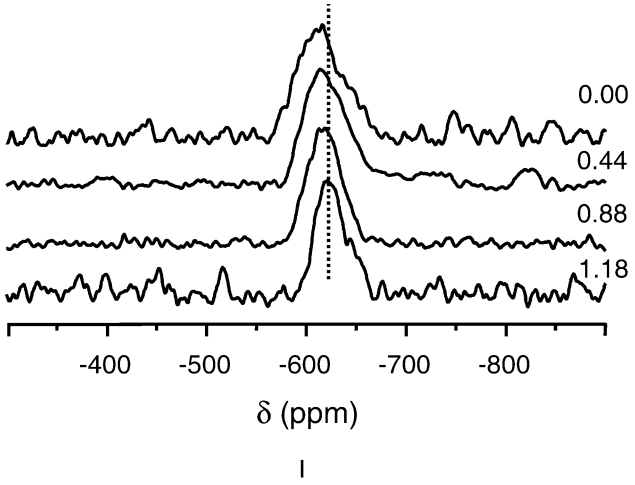

Fig. 5. 119Sn MAS NMR spectra of selected $(Sn_{1.6-x}Pb_x)(Nb_{2-y}Sn_y)O_{6.6-0.5y}$ samples (the x value is depicted). Around 10,000 transients have been accumulated for each sample.

^{93}Nb MAS NMR single-quantum spectra of selected $(Sn_{1.6-x}Pb_x)(Nb_{2-y}Sn_y)O_{6.6-0.5y}$ samples (Fig. 6) display an asymmetric peak which broadens with increasing tin content. The ^{93}Nb MAS NMR triple-quantum spectra depicted in Fig. 7 clearly show the presence of, at least, two distinct niobium sites, S1 and S2. Simulation of the single- (Fig. 6) and triple-quantum (Fig. 7) ^{93}Nb MAS NMR spectra using the same set of quadrupole parameters, collected in Table 9, indicates that the populations of sites S1 and S2 are always in a ca. 2:1 intensity ratio, respectively. However, as the tin content

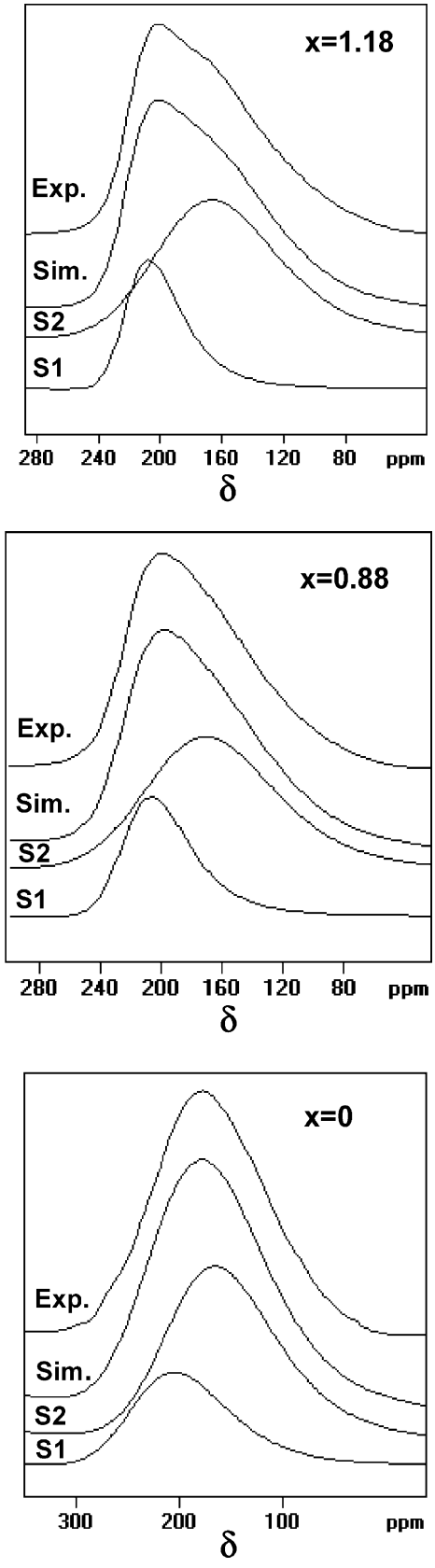

Fig. 6. Experimental and simulated single-quantum ^{93}Nb MAS NMR spectra of selected $(Sn_{1.6-x}Pb_x)(Nb_{2-y}Sn_y)O_{6.6-0.5y}$ samples (the x value is depicted).

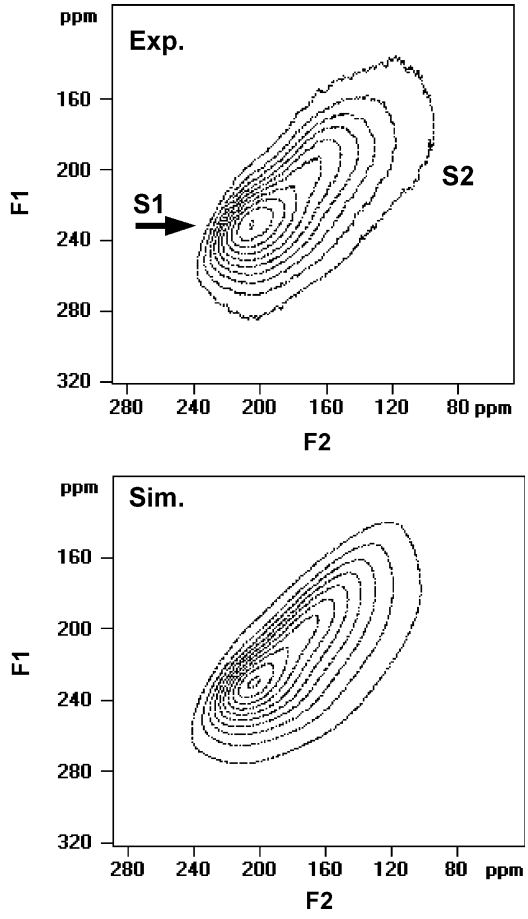

Fig. 7. Experimental and simulated triple-quantum ^{93}Nb MAS NMR spectrum of $Sn_{0.06}(II)Pb_{1.18}Nb_{1.66}Sn(IV)_{0.34}O_{6.07}$.

increases the average quadrupole coupling constants of both sites increase significantly, from ca. 14.4 (S1) and 17.8 (S2) MHz for $x = 1.18$, to ca. 22.8 (S1) and 23.6 (S2) MHz for $x = 0$. Although site S2 is more distributed (quadrupole coupling constant and isotropic chemical shift) than S1, tin insertion results in a larger parameter distribution increase for S1. The observed increase of ^{93}Nb quadrupole coupling constant upon tin insertion is consistent with the results of the structure refinements. The ^{93}Nb surrounding is different, looking at the tin or lead nearest neighbors. There are six Nb–Pb distances of equal length (3.7 Å). There are also six Nb–Sn distances but they are distributed over four bond-lengths (from 3.02 to 4.45 Å). However, as stressed above, these are average distances and, if lead and tin are shifted from the found positions in the [110] direction, the number of distances must be multiplied by a factor of, at least, two (though the length of these distances cannot vary too much from the observed average values). In summary, introducing more tin atoms in the neighborhood of niobium generates larger electric field gradients at the site of the ^{93}Nb nucleus (larger C_Q values) and creates a distribution of local environments. From this reasoning it also follows that

Table 9
Quadrupole coupling parameters of ^{93}Nb sites

x	Site S1				Site S2			
	δ_{iso} (ppm)	$\Delta\delta_{iso}$ (ppm)	C_Q (MHz)	ΔC_Q (MHz)	δ_{iso} (ppm)	$\Delta\delta_{iso}$ (ppm)	C_Q (MHz)	ΔC_Q (MHz)
0	247	25	22.8	11.9	212	35	23.6	12.3
0.88	224	14.5	15.3	8.0	201	33.0	18.2	9.5
1.18	221	10.0	14.4	7.5	193	30.0	17.8	9.3

δ_{iso}—average isotropic chemical shift; $\Delta\delta_{iso}$—isotropic chemical shift distribution; C_Q—average quadrupole coupling constant; ΔC_Q—quadrupole coupling constant distribution.
Notes: S1:S2 populations are all in a 1:2 ratio; asymmetry parameter η has been set to 0.65.

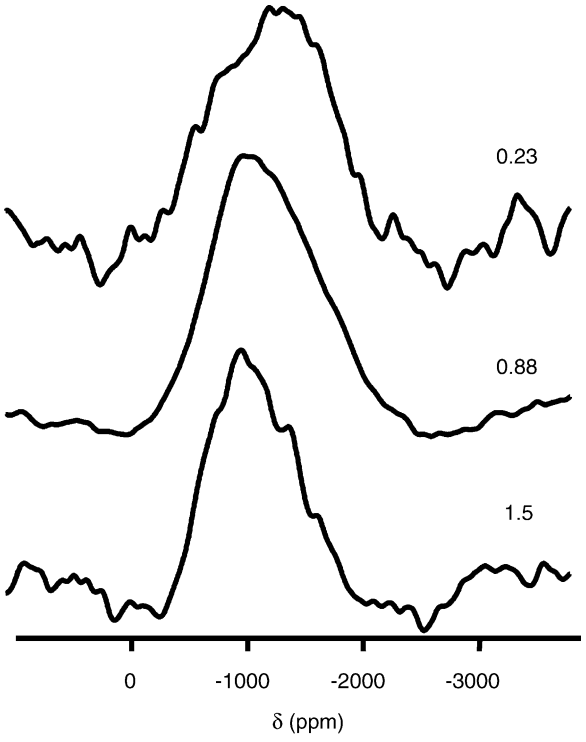

Fig. 8. Static ^{207}Pb NMR spectra of $(Sn_{1.6-x}Pb_x)(Nb_{2-y}Sn_y)O_{6.6-0.5y}$ samples (the x value is depicted). Around 30,000 transients have been accumulated for each sample.

an increase in chemical shift dispersion is also expected. However, the structure model does not explain why two types of niobium sites are present. One possibility is that they arise due to the presence of different domains in the sample, as previously reported for PMN [19,20]. This hypothesis will have to be confirmed, or otherwise, by future (e.g., TEM) studies.

Static ^{207}Pb NMR spectra of selected $(Sn_{1.6-x}Pb_x)(Nb_{2-y}Sn_y)O_{6.6-0.5y}$ samples (Fig. 8) display very broad asymmetric lines with an FWHM which increases from ca. 920 ppm (sample A11, $Sn_{0.07}Pb_{1.5}Nb_{1.83}Sn_{0.17}O_{6.48}$) to 1400 ppm (A2, $Sn_{1.42}Pb_{0.23}Nb_{1.87}Sn_{0.13}O_{6.59}$) with increasing tin content. This is probably due to both increasing chemical shift anisotropy and a distribution of chemical shifts. Although empirical correlations between anisotropy and structure based on average deviation of bond angles or bond lengths from that of a perfect polyhedron yield poor results for lead, the large spans of ^{207}Pb NMR spectra show its sensitivity to slight deviations from spherical symmetry [21].

In conclusion, we have prepared mixed lead and tin niobates of the pyrochlore type, described by the formula $(Sn_{1.6-x}Pb_x)(Nb_{2-y}Sn_y)O_{6.6-0.5y}$, where x (0–1.6) is the Pb(II) and y (0–0.34) is the Sn(IV) contents. Here we described the synthesis and crystal structure of these new compounds. In a forthcoming paper, we shall report on their electric properties. Preliminary results indicate that these materials exhibit dielectric properties in the range 73–473 K.

References

[1] W.R. Cook, H. Jaffe, Phys. Rev. 88 (1952) 1426.
[2] W.R. Cook, H. Jaffe, Phys. Rev. 88 (1953) 1297.
[3] F. Brisse, O. Knop, Can. J. Chem. 46 (1968) 859.
[4] J.L. Fourquet, H. Duroy, Ph. Lacorre, J. Solid State Chem. 114 (1995) 575.
[5] B.J. Ismunandar, B.A. Kennedy, T. Hunter, Vogt, J. Solid State Chem. 131 (1997) 317.
[6] R.A. Beyerlein, H.S. Horowitz, J.M. Longo, M.E. Leonowicz, J. Solid State Chem. 51 (1984) 253.
[7] I. Radosavljevic, J.S.O. Evans, A.W. Sleight, J. Solid State Chem. 136 (1998) 63.
[8] K. Sreedhar, A. Mitra, J. Am. Ceram. Soc. 82 (1999) 1070.
[9] P. Cerny, A.-M. Fransolet, T.S. Ercit, R. Chapman, Can. Miner. 26 (1988) 889.
[10] L.P. Cruz, J.–M. Savariault, J. Rocha, J.-C. Dumas, J.D. Pedrosa de Jesus, J. Solid State Chem. 156 (2001) 349.
[11] T. Birchall, A.W. Sleigth, J. Solid State Chem. 13 (1975) 118.
[12] C. Fernandez, A.A. Quoineaud, V. Montouillout, S. Gautier, S. Lacombe, in: A. Galarneau, et al. (Eds.), Studies in Surface Science and Catalysis, Vol. 135, Elsevier, Amsterdam, 2001, p. 183.
[13] D. Le Bellac, J.M. Kiat, P. Garnier, H. Moudden, Ph. Sciau, P.A. Buffat, G. André, Phys. Rev. B 52 (1995) 13–184.
[14] L.P. Cruz, J.-M. Savariault, J. Rocha, Acta Crystallogr. C 57 (2001) 1001.
[15] J. Rodriguez-Carvajal, FULLPROF Program for Rietveld Refinement and Pattern Matching Analysis, Abstracts of the Satellite Meeting on Powder Diffraction of the XVth Congress of the International Union of Crystallography, Toulouse, France, 1990.

[16] G.M. Sheldrick, SHELXL97 Program for the Refinement of Crystal Structures, University of Göttingen, Germany, 1997.
[17] J. Galy, G. Meunier, S. Andersson, A. Åström, J. Solid State Chem. 13 (1975) 142.
[18] D. Altermatt, I.D. Brown, Acta Crystallogr. B 41 (1985) 240.
[19] L.P. Cruz, J. Rocha, J.D. Pedrosa de Jesus, J.M. Savariault, J. Galy, Solid State NMR 15 (1999) 153.
[20] J.J. Fitzgerald, S. Prasad, J. Huang, J.S. Shore, J. Am. Chem. Soc. 122 (2000) 2556.
[21] F. Fayon, I. Farnan, C. Bessada, J. Coutures, D. Massiot, J.P. Coutures, J. Am. Chem. Soc. 119 (1997) 6837.